

1                   **Historic carbon burial spike in an Amazon floodplain lake linked to riparian**  
2   **deforestation near Santarem, Brazil**  
3  
4  
5  
6  
7

8   Luciana M. Sanders<sup>1</sup>, Kathryn Taffs<sup>1</sup>, Debra Stokes<sup>2</sup>, Christian J. Sanders<sup>3</sup>, Alex Enrich-  
9   Prast<sup>4,5</sup>, Leonardo Nogueira Amora<sup>6,7</sup>, Humberto Marotta<sup>6,7</sup>

10  
11   <sup>1</sup>*School of Environment, Science and Engineering, Southern Cross University, Coffs Harbour, New South*  
12                   *Wales, Australia.*

13   <sup>2</sup>*Marine Ecology Research Centre, Southern Cross University, P.O. Box 157, Lismore, NSW 2480, Australia*  
14   *University, P.O. Box 157, Lismore, NSW 2480, Australia*

15   <sup>3</sup>*National Marine Science Centre, School of Environment, Science and Engineering, Southern Cross*  
16                   *University, Coffs Harbour, New South Wales, Australia..*

17   <sup>4</sup>*Laboratório de Biogeoquímica, Universidade Federal do Rio de Janeiro (UFRJ), Rio d Janeiro (RJ),*  
18                   *21941 971, Brazil.*

19   <sup>5</sup>*Department of Environmental Change, Linköping University, 581 83, Linköping, Sweden.*

20   <sup>6</sup>*Ecosystems and Global Change Laboratory (LEMG-UFF) / International Laboratory of Global Change*  
21                   *(LINCGlobal). Biomass and Water Management Research Center (NAB-UFF). Graduated Program in*  
22                   *Geosciences (Environmental Geochemistry). Universidade Federal Fluminense (UFF), Av. Edmundo*  
23                   *March, s/n° – Zip Code: 24210-310, Niteroi/RJ- Brazil.*

24   <sup>7</sup>*Sedimentary and Environmental Processes Laboratory (LAPSA-UFF). Department of Geography.*  
25                   *Graduated Program in Geography. Universidade Federal Fluminense (UFF), Av. Gal. Milton Tavares*  
26                   *de Souza, s/n° - Zip Code: 24210-346, Niteroi/RJ- Brazil.*

27  
28   \*Corresponding author. E-mail address; [l.sanders.13@student.scu.edu.au](mailto:l.sanders.13@student.scu.edu.au)  
29  
30  
31  
32

33

34 **Abstract**

35 Forests along the Amazon Basin produce significant quantities of organic material, a  
36 portion of which is deposited in floodplain lakes. Deforestation in the watershed may then have  
37 potentially important effects on the carbon fluxes. In this study, a sediment core was extracted  
38 from an Amazon floodplain lake to examine the relationship between carbon burial and  
39 changing land cover/land use. Historical records from the 1930s and satellite data from the  
40 1970s were used to calculate deforestation rates between 1930 and 1970, and 1970 to 2010 in  
41 four zones with different distances from the margins of the lake and its tributaries (100, 500,  
42 1000 and 6000 m buffers). A sediment accumulation rate of  $\sim 4 \text{ mm year}^{-1}$  for the previous  $\sim 120$   
43 years was determined from the  $^{240+239}\text{Pu}$  signatures and the excess  $^{210}\text{Pb}$  method. The carbon  
44 burial rates ranged between 85 and 298  $\text{g C m}^{-2} \text{ year}^{-1}$ , with pulses of high carbon burial in the  
45 1950s, originating from the forest vegetation as indicated by  $\delta^{13}\text{C}$  and  $\delta^{15}\text{N}$  signatures. Our  
46 results revealed a potentially important spatial dependence of the OC burial in Amazon  
47 lacustrine sediments in relation to deforestation rates in the catchment. These deforestation  
48 rates were more intense in the riparian vegetation (100 m buffer) during the period 1930 to  
49 1970 and the larger open water areas (500, 1000 and 6000 m buffer) during 1970 to 2010. The  
50 continued removal of vegetation from the interior of the forest was not related to the peak of  
51 OC burial in the lake, but only the riparian deforestation which peaked during the 1950s.  
52 Therefore, this supports the conservation priority of riparian forests as an important  
53 management practice for Amazon flooded areas. Our findings suggest the importance of abrupt  
54 and temporary events in which some of the biomass released by the deforestation, especially  
55 restricted to areas along open water edges, might reach the depositional environments in the  
56 floodplain of the Amazon Basin.

57

58

59 **1. Introduction**

60 Rivers act as vectors, transporting sediment from land to ocean (Abril et al. 2014). Along  
61 this trajectory a significant proportion of the sediment load, including organic material, may be  
62 deposited in floodplains, creating zones of carbon accumulation (Smith et al. 2002, Dong et al.  
63 2012, Hoffmann et al. 2013). This process is accelerated during flood events, when rivers and  
64 tributaries deposit organic material along the inundated floodplains (Smith et al. 2002). In some  
65 climate zones, floodplains are seasonally inundated, with riparian zone vegetation dependent  
66 upon this seasonal influx of organic material. The riparian vegetation slows water velocity and  
67 traps fine-grained, carbon rich sediments within this low-energy environment (Aalto et al.  
68 2003). Therefore, the riparian vegetation along the floodplains may be important for the organic  
69 matter deposition and the Amazon carbon cycle.

70 The importance of tropical wetland ecosystems in the carbon cycle is well documented  
71 (Downing et al. 1993, Melack et al. 2004, Zocatelli et al. 2013, Abril et al. 2014, Marotta et al.  
72 2014). It has been shown that wetlands in the warm tropics are some of the most productive  
73 biological communities in the world (Neue et al. 1997), representing an important sink for  
74 nutrients (Marotta et al. 2009) and carbon (Peixoto et al. 2016, Sanders et al. 2017), as well as  
75 sources of organic substrates to carbon gas production in inland waters (Marotta et al. 2010).  
76 However, these wetland ecosystems are also highly threatened by land use activities, especially  
77 from deforestation, development of agricultural land and soil degradation (Junk 2013, Lucas et  
78 al. 2014).

79 The Amazon Basin wetlands are being degraded by farming activities such as commercial  
80 ranching and an increase in road density (Goulding 1993). Deforestation of the Amazon Basin  
81 commenced ~ 1930 and accelerated toward the end of the 1970's (Skole and Tucker 1993),  
82 when an estimated 15% of the pristine rainforest area was lost by the year 2003, increasing to  
83 approximately 18% by 2015 (INPE 2016). The ongoing loss of vegetation is responsible for a  
84 substantial increase in erosion rates and subsequent sediment inputs into Amazon rivers and

85 lakes (Neill et al. 2013b). Yet these anthropogenic activities are potential sources of  
86 allochthonous organic matter that may increase carbon stores in the associated floodplain areas  
87 (Diaz and Rosenberg 2008, Stanley et al. 2012).

88 Jupindá Lake, in the state of Pará, provides an ideal opportunity to investigate historical  
89 changes in organic carbon burial in a floodplain lake as a result of the well documented  
90 anthropogenic activities within its watershed. This will aid in identifying the little known  
91 impacts of land cover changes on recent carbon burial rates in depositional environments of  
92 the Amazon floodplain. The objectives of this research are to investigate the effects of  
93 deforestation and urban development on carbon burial rates in a tropical floodplain lake. We  
94 hypothesize that the historical deforestation in this region of the Amazon may have influenced  
95 the OC burial rates in the studied floodplain lake.

96

## 97 **2. Methods**

98 The city of Santarém, in central Amazon, was established in the mid-eighteenth century,  
99 approximately 650 km upstream from the Amazon River mouth and at its confluence with the  
100 Tapajós River (02°25'0.28"S and 54°42'41.57"W, Figure 1). In 1940, Santarém was only a  
101 small village, less than 0.5 km<sup>2</sup>, surrounded by dense pristine rainforest (estimated from the  
102 historical mapping of the Santarém City Hall). This city quickly expanded, occupying 5.2 km<sup>2</sup>  
103 by the end of the 1970s and 49.3 km<sup>2</sup> currently (estimated from satellite images  
104 LANDSAT/SRTM). Jupindá Lake is 70 km east of Santarém City, and receives surface water  
105 inflow from small streams draining from the forest and the main tributary Curuá-Una River, a  
106 large affluent of the Amazon River (Figure 1). The Lake has been affected by the deforestation  
107 associated with the expansion of Santarém City. Between the 1940's and 1950's, there was  
108 intense deforestation on the margins of rivers and streams in this area, used to supply the  
109 markets with wood and forestry products (Amorim 2000, Cruz et al. 2011). In the 1970s, the

110 Curuá-Una River was dammed (Curuá-Una Dam) 45 km upstream of Jupindá Lake to build  
111 the first hydroelectric plant of the Amazon Forest (Ligocki 2003).

112 A 60 cm sediment core (diameter 7.5 cm) was collected in 2010 using a gravity corer in the  
113 center of the Jupindá Lake (02°27'43.60" S, 54° 5'1.30" W). The sediment core was sub  
114 sampled at 2 cm intervals. Dry bulk density (DBD,  $\text{g cm}^{-3}$ ) was determined as the dry sediment  
115 weight (g) divided by the initial volume ( $\text{cm}^3$ ). A homogenized portion was acidified (10%  
116 HCl following the procedures outlined in Naidu et al. (2000)) to remove carbonate material,  
117 then dried and ground to powder for organic carbon (OC), nitrogen (N),  $\delta^{13}\text{C}$ , and  $\delta^{15}\text{N}$  analyses  
118 using a Flash Elemental Analyzer coupled to a Thermo Fisher Delta V IRMS (isotope ratio  
119 mass spectrometer). The  $\delta^{15}\text{N}$  results and the C/N ratios results should be interpreted with  
120 caution, based on this pre-treatment method, which may be influenced by the composition of  
121 the bulk organic matter (Brodie et al. 2011). Working standards were used (glucose, 10.7 ppt  
122 and urea, 41.3 ppt) to calibrate for  $\delta^{13}\text{C}$ . A pair of standards was measured with every 20  
123 samples. These standards were calibrated initially against international absolute standards  
124 LSVEC and NIST8542. Analytical precision: C = 0.1 %, N = 0.1%,  $\delta^{13}\text{C}$  = 0.1‰ and  $\delta^{15}\text{N}$  =  
125 0.15 ‰.

126 Samples were prepared for Pu dating following the method of Ketterer et al. (2004) with  
127 modifications to enable larger sample mass to be processed as a result of the likely lower Pu  
128 concentrations in the Southern Hemisphere (Sanders et al. 2016). To obtain a larger mass,  
129 sediment intervals were joined and homogenized so the sediment intervals for the  $^{240+239}\text{Pu}$   
130 dating was 4 cm intervals. Sample aliquots ranging from 14 to 29 grams were dry-ashed at 600  
131 °C for 16 hours, and leached with 50 mL of 16 M  $\text{HNO}_3$ . The leaching was conducted overnight  
132 at 80°C with added  $^{242}\text{Pu}$  yield tracer (NIST 4334g, 19 picograms). Acid leaching (as opposed  
133 to complete dissolution with HF) is known to solubilize stratospheric fallout Pu, and there is  
134 little possibility that “refractory”  $\text{HNO}_3$ -insoluble Pu exists in the South America (Sanders et

135 al. 2014). The leachates were diluted to 100 mL, filtered to remove solids, and the aqueous  
136 solutions were processed with TEVA resin (EiChrom, Lisle, IL, USA) in order to chemically  
137 isolate 3.0 mL Pu fractions in aqueous ammonium oxalate solution suitable for measurements  
138 by sector ICPMS. Pu determinations were performed using a VG Axiom MC operating in the  
139 single collector (electron multiplier) mode. The system was used with an APEX HF desolvating  
140 micronebulizer system (ESI Scientific, Omaha, NE, USA) with an uptake rate of 0.4  
141 mL/minute. Qualitative mass spectral scans (averages of 50 sweeps over the mass range 237.4  
142 – 242.6) were collected for selected samples prior to the electrostatic sector quantitative  
143 scanning of  $^{238}\text{U}^+$ ,  $^{239}\text{Pu}^+$ ,  $^{240}\text{Pu}^+$ , and  $^{242}\text{Pu}^+$ . Detection limits were evaluated based upon the  
144 analysis of two blanks and considerations regarding the obtained mass spectra. A detection  
145 limit of 0.01 Bq/kg of  $^{239+240}\text{Pu}$  is applicable for samples of nominal 25 g mass.

146 For  $^{210}\text{Pb}$  dating, an intrinsic germanium detector coupled to a multi-channel analyzer was  
147 used. Freeze dried and ground sediments were packed and sealed in gamma tubes. Lead-210  
148 and  $^{226}\text{Ra}$  activities were calculated by multiplying the counts per minute by a factor that  
149 includes the gamma-ray intensity and detector efficiency determined from standard  
150 calibrations. Identical geometry was used for all samples. Lead-210 activities were determined  
151 by the direct measurement of the 46.5 KeV gamma peak. Radium-226 activity was determined  
152 via the  $^{214}\text{Pb}$  daughter at 351.9 KeV. For  $^{226}\text{Ra}$  measurements, the packed samples were set  
153 aside for at least 21 days to allow for  $^{222}\text{Rn}$  to ingrow and establish secular equilibrium between  
154  $^{226}\text{Ra}$  and its granddaughter  $^{214}\text{Pb}$ . Excess  $^{210}\text{Pb}$  activity was calculated by subtracting the  
155 supported  $^{210}\text{Pb}$  (i.e.,  $^{226}\text{Ra}$  activity) from the total  $^{210}\text{Pb}$  activity. The sediment accretion rate  
156 for the previous 120 years was estimated by two methods derived from  $^{210}\text{Pb}$  dating, the  
157 Constant Initial Concentration (CIC) model assuming that this rate has not varied during the  
158 encompassed time span (Appleby and Oldfield 1992), and the Constant Rate of Supply (CRS)  
159 model based on a constant influx of unsupported, atmospheric  $^{210}\text{Pb}$  that allows a variable

160 sediment rate (Ivanovich and Harmon 1992). Organic carbon accumulation rates were  
161 estimated from an average between these the two dating methods ( $^{239+240}\text{Pu}$  and  $^{210}\text{Pb}_{\text{ex}}$ ), the  
162 dry bulk density ( $\text{g cm}^3$ ) and carbon content for each interval of the entire sediment core.

163 The land use and land cover analysis was based on documented historical information  
164 before 1975 and satellite images (Landsat/SRTM, Table 1) from 1975, 1985, 1995 and 2008  
165 available from the United States Geological Survey (USGS). No significant deforestation  
166 occurred in the catchment area of the Jupindá Lake until the early 1940's (Amorim 2000, Cruz  
167 et al. 2011). Subsequent land/use changes were determined using satellite images (Gordon  
168 1980, Munyati 2000). All satellite images were from low-water seasons to remove the influence  
169 of the flood pulse on the exposed area over years. The resolution of the images was 30 m,  
170 except that from the 1970's, which was resampled from 90 to 30 m (Table 1). This approach  
171 allowed an assessment of changes in land cover could then be compared to results from carbon  
172 accumulation. Results of the spatial assessment were separated into two time periods; 1930 to  
173 1970, the timeframe between the onset of land clearing and the first satellite image, and 1970  
174 to 2010 which provides a more detailed assessment of temporal changes to the study area. The  
175 time period 1930 to 1970 was characterized by a rapid removal (peak until the 1960's) of  
176 vegetation established at the margins of inland waters; especially *Aniba rosaeodora* (Pau-rosa)  
177 for extraction of oils, and *Mezilaurus itauba* and *Cedrela fissilis* (Louro-itaúba and Cedro,  
178 respectively) as hardwoods, and the opening of clearings for crops of textile fibers and  
179 subsistence products. Intensification of deforestation towards the interior of the forest and  
180 following the urban growth of Santarém is reported from the 1970's (Amorim 2000, Cruz et  
181 al. 2011). The depletion of vegetation near to the margins of lakes and running waters in this  
182 region is also well documented (Amorim 2000, Cruz et al. 2011).

183 In order to address the spatial dependence of recent OC burial in Jupindá Lake for  
184 deforestation, we analyzed the land cover and land use in four buffer areas around the lake and

185 contributing rivers or streams. The first buffer of 100 m represented the riparian forest protected  
186 area by the Brazilian laws for fluvial channels with a width of 50 to 200 m. Other buffers were  
187 progressively higher, with a width of 500, 1000 and 6000 m from the riverbank and lake  
188 margins (Figure 2). In addition, we considered only stretches of rivers and streams 65 km long  
189 from Jupindá Lake to analyze its catchment area of more direct influence. This criteria also  
190 avoids the interference of the artificial flooding on the margins of the Curuá-Una hydroelectric  
191 dam, which was built in 1977 (Fearnside 2005).

192 The statistical treatment of variables and OC burial rates, when grouped into different  
193 phases, showed assumptions which required parametric analyses, including normal  
194 distribution (Kolmogorov-Smirnov,  $p > 0.05$ ) and homogeneity of variance (Bartlett,  $p > 0.05$ ).  
195 Thus, we used means and standard errors to represent the distribution of values, and parametric  
196 tests were conducted, allowing comparison of different phases. Statistical differences were  
197 tested using the one-way ANOVA test followed by Tukey's post test (significance was defined  
198 as  $p < 0.05$ ). All the statistical tests used in this work were performed using GraphPad Prism  
199 5.0 software.

200

### 201 3. Results

202 The analyses of  $^{239+240}\text{Pu}$  showed no detectable activities from the base of the sediment core  
203 until the 22-26 cm interval (Figure 3). However,  $^{239+240}\text{Pu}$  was detected in the 18-22 cm interval  
204 ( $0.029 \pm 0.002 \text{ Bq/kg } ^{239+240}\text{Pu}$ ) with the peak concentration ( $0.047 \pm 0.004 \text{ Bq/kg } ^{239+240}\text{Pu}$ ) at  
205 the 16 cm depth, which indicates the 1963 stratospheric fallout peak. Hence material below 22  
206 cm was deposited pre-bomb (that is, prior to the early 1950's). This affixes an upper limit on  
207 the average sedimentation rate of near to  $3.8 \text{ mm year}^{-1}$ . The Pu atom ratio data indicate that  
208 the Pu is originating from stratospheric fallout with isotopic ratios ( $^{240/239}\text{Pu}$ ) of  $\sim 0.18$ . These  
209 results are consistent with the  $^{240}\text{Pu}/^{239}\text{Pu}$  of  $0.180 \pm 0.014$  discussed by Kelley et al. (1999).



210 The  $^{210}\text{Pb}$  and  $^{226}\text{Ra}$  profiles as well as the  $^{210}\text{Pb}_{\text{(ex)}}$  profile vs cumulative dry mass  
211 accumulation reveals a complex depositional environment with sedimentation variations and  
212 disturbances, such as bioturbation and resuspension in the upper ~ 20 cm of the sediment  
213 column (Figure 4). A decrease in  $^{210}\text{Pb}_{\text{ex}}$  activity was found below the 20 cm depth interval.  
214 The  $^{210}\text{Pb}_{\text{ex}}$  data distribution are as follows:  $y = -0.0749x + 7.5$ ;  $R^2 = 0.73$ ;  $n=19$ ;  $p < 0.01$  from  
215 the 20 to the 60 cm interval, below the apparent mixed zone. Both estimates of sediment  
216 accretion rate during the 120 years from CIC and CRS models were similar, reaching 4.1 and  
217  $4.3 \text{ mm yr}^{-1}$  respectively, which were slightly higher than the ~ 60 year  $^{239+240}\text{Pu}$  dates ( $3.8 \text{ mm}$   
218  $\text{yr}^{-1}$ ). In order to obtain a more reliable estimates of the historical carbon burial rates, the  
219  $^{239+240}\text{Pu}$  results, from near 1950 to present, were used ( $3.8 \text{ mm year}^{-1}$ ) and  $^{210}\text{Pb}_{\text{ex}}$  ( $4.2 \text{ mm}$   
220  $\text{year}^{-1}$ ) was used from ~1890 to approximately the 1950s. These rates for each sediment depth  
221 were multiplied by the DBD and OC content for each interval of the entire sediment core.

222 The dry bulk density (DBD), total organic carbon (OC%), total nitrogen (TN%) content as  
223 well as the carbon and nitrogen (C/N) molar ratios along with the  $\delta^{13}\text{C}$  and  $\delta^{15}\text{N}$  values showed  
224 a decreasing shift towards the center of the sediment core (Table 2). The relationship between  
225  $\delta^{13}\text{C}$  and  $\delta^{15}\text{N}$  indicated different origins of OC in the sediment core (Figure 5) contributing to  
226 the significant relationship between OC burial and the  $\delta^{13}\text{C}$  (Figure 6). The significantly greater  
227  $\delta^{13}\text{C}$  peak and lower  $\delta^{15}\text{N}$  values coupled to higher OC burial rates were observed in the phase  
228 between ~1930 to 1970 in Jupindá Lake (one-way ANOVA followed by Tukey's post test,  
229  $p < 0.05$ ; Fig. 7). The  $\delta^{13}\text{C}$  values were greater in the phase ~1930 to 1970 in relation to those  
230 previous and after respectively (one-way ANOVA followed by Tukey's post test,  $p < 0.05$ ). This  
231 peak near 1950 also showed  $\delta^{15}\text{N}$  values lower and OC burial rates higher than other  
232 phases (one-way ANOVA followed by Tukey's post test,  $p < 0.05$ ).

233 The OC burial rates indicate an increasing trend from ~ 1930 with a peak during the 1940's  
234 and 50's (Figure 7). The carbon burial rates increased from ~ $186 \text{ g m}^{-2} \text{ year}^{-1}$  before the 1950s,

235 and up to 298 g m<sup>-2</sup> year<sup>-1</sup> between the 1940s and 1950s. Carbon accumulation then decreased  
236 to approximately 186 g m<sup>-2</sup> year<sup>-1</sup> from 1960 to 1980, after which a gradual decline in carbon  
237 burial is noted. In relation to land use/cover in the surrounding fluvial channels and the Jupindá  
238 Lake, only the smallest buffer (100 m) showed significant changes during 1930-1970. This  
239 time period is when deforestation was nearly 75% higher than in the subsequent time period  
240 1970-2010 (Figure 8a) and when OC burial was greatest (Figure 8b).

241

#### 242 **4. Discussion**

243 Similar estimates of sediment accretion were calculated using different methodologies  
244 (<sup>239+240</sup>Pu and <sup>210</sup>Pb<sub>(ex)</sub>). These accretion rates along with the dry bulk density revealed an  
245 insight into changes in the sediment sources of floodplains, and their relationships with  
246 changing land cover and land use in the Amazon Basin. The Jupindá Lake showed substantial  
247 changes in the carbon burial rates following deforestation, supporting the connection between  
248 flooded areas and their surrounding vegetation. The high peak in carbon accumulation observed  
249 around 1950 appears to be associated with a shift in the source of organic material, inferred by  
250 changes in carbon and nitrogen contents and the isotopic fractioning toward the middle (from  
251 20 to 40 cm depth interval) of the sediment column. This peak for different organic and  
252 inorganic variables in intermediate depths revealed changes not only in the amount but also in  
253 the type of material being deposited over time. Previous studies have reported two common  
254 origins for OC in the Amazon forest. Higher  $\delta^{15}\text{N}$  and more negative  $\delta^{13}\text{C}$  values could indicate  
255 the presence of Santarém soil organic matter (such as that adjacent to the Jupindá Lake), while  
256 lower  $\delta^{15}\text{N}$  and more variable  $\delta^{13}\text{C}$  values indicate particulate organic carbon (POC) from the  
257 terrestrial vegetation in the catchment (Ometto et al. 2006, Zocatelli et al. 2013). Here, a  
258 corresponding increase in OC%, TN% and OC burial rates measured, with a peak near 1950,  
259 suggesting higher inputs of organic matter into lake. The higher  $\delta^{13}\text{C}$  signature, coupled with a

260 lower  $\delta^{15}\text{N}$  indicates a greater influence from the terrestrial Amazonian POC during the same  
261 period, around 1950 (Ometto et al., 2006).

262 When looking for a cause for this change in the source of organic material, we look to the  
263 analysis of land use change. Land clearing associated with early occupation from the 1940s in  
264 the catchment area of the Jupindá Lake may be a potential cause of the increased carbon burial  
265 observed in the lake. Changes in land use and associated deforestation may significantly affect  
266 OC burial in mid-high-latitude lakes (Anderson et al. 2013, Dietz et al. 2015). Indeed, our  
267 results suggest that land clearing during the 1940's and 50's might be related to increased  
268 organic matter deposition in the region's floodplain lakes. During this period, intense wood  
269 extraction and expansion of agricultural settlements occurred (Amorim 2000, Cruz et al. 2011).  
270 One important consequence of deforestation in the watershed is the silting up of lakes (Enea et  
271 al. 2012 ), including those at humid low-latitude areas (Cohen et al. 2005, Bakoariniaina et al.  
272 2006). However, the lake is in a region relatively well protected, and therefore there is no other  
273 explanation other than deforestation in the margins to have caused the peak in OC burial near  
274 the 1950s. The riparian forest systems are generally effective in reducing the sediment transport  
275 by surface runoff, with the removal of this vegetation increasing the erosion processes,  
276 especially in the Amazon Basin as a result of intense rainfall (Neill et al. 2013a). The peak of  
277 the significantly greater  $\delta^{13}\text{C}$  and lower  $\delta^{15}\text{N}$  values coupled to higher OC burial rates were  
278 observed in the phase between ~1930 to 1970 in Jupindá Lake (one-way ANOVA followed by  
279 Tukey's post test,  $p < 0.05$ ; Fig. 7). The  $\delta^{13}\text{C}$  values were greater in the ~1930 to 1970 phase as  
280 related to those previous and after respectively (one-way ANOVA followed by Tukey's post  
281 test,  $p < 0.05$ ). This peak between ~1930 to 1970 also showed delta  $\delta^{15}\text{N}$  values lower and OC  
282 burial rates higher than other phases (one-way ANOVA followed by Tukey's post test,  
283  $p < 0.05$ ).

284 We also found a spatial dependence of the carbon accumulation in Lake Jupindá, as the  
285 much lower OC burial was coupled to higher deforestation rates in those larger buffers around  
286 its margins and main fluvial channels (500, 1000 and 6000 m) in the period after 1970s  
287 (between the 1970s to 2010) than that before (~1930 to 1970). This confirms previous evidence  
288 that the recent deforestation process in the region commenced in the riparian zone (Amorim  
289 2000, Cruz et al. 2011), and not in the interior of the forest. The enhanced OC burial in  
290 lacustrine sediments before ~1970 was related to higher deforestation rates only in the riparian  
291 vegetation zone (100 m buffers), suggesting a higher influence of deforestation with decreasing  
292 distance to water courses. Therefore, the soil carbon enrichment to the aquatic sediments during  
293 the peaks of riparian deforestation may cause intense but temporary carbon burial events in the  
294 Amazon floodplain, representing potentially only a significant part of the total loss of terrestrial  
295 organic matter. In addition, the continued removal of vegetation from the interior of the forest  
296 might not be directly related to increases of OC burial, even temporarily, in depositional aquatic  
297 ecosystems.

298

## 299 **5. Conclusion**

300 Palaeolimnological techniques were used with a historical spatial analysis of deforestation  
301 to interpret changes in sediment characteristics during the past century. The Pu dating method  
302 closely approximates measurements from the  $^{210}\text{Pb}$  chronologies and hence offers a technique  
303 to determine sedimentation rates and carbon accumulation in Amazon sediments. An increase  
304 in OC burial, up to 298 OC g m<sup>-2</sup> year<sup>-1</sup>, coincides with changes in the  $\delta^{13}\text{C}$  and  $\delta^{15}\text{N}$  signatures,  
305 likely influenced by the heavy deforestation in riparian systems of this region during the 1940s  
306 and 1950s. It is suggested that the net increase in carbon burial towards the center of the  
307 sediment core, which represents the highest carbon burial rates during the 1950s, is a result of  
308 a change in source of organic matter deposition. However, any increase of OC burial rates

309 attributed to deforestation might be lower than the loss of terrestrial biomass in the standing  
310 crop or soils. The differing carbon burial rates along the sediment core therefore identify the  
311 potential complexity of the Amazon floodplain lakes, directly related to the development within  
312 the Basin. This work supports the urgent need for management practices based on the  
313 conservation of riparian forests, demonstrating the spatial dependence of carbon burial capacity  
314 of the Amazon floodplain lakes with respect to advances in deforestation in the Basin.

315

### 316 **Acknowledgements**

317 LMS is supported by an APA and IPRS scholarships. HM received a research grant from the  
318 Brazilian Research Council (CNPq – “Programa Universal”) and the Research Support  
319 Foundation of the State of Rio de Janeiro (FAPERJ – “Programa Jovem Cientista do Nosso  
320 Estado”). CJS is supported by the Australian Research Council (DE160100443).

321

322

### 323 **CAPTIONS TO FIGURES**

324 **Figure 1.** Jupindá Lake where the sediment core was extracted, near the Amazon River and  
325 the city of Santarém, Brazil. This floodplain lake has a diameter of approximately 3 km.

326 **Figure 2.** Different buffer sizes (100 m, 500 m, 1 km and 6 km) along the stretch of the  
327 Curuá-Una River from Jupindá Lake (red) to the hydroelectric dam upstream (yellow).

328 **Figure 3.**  $^{239+240}\text{Pu}$  profile, indicating ~ 1950 when these radionuclides were first introduced  
329 into the atmosphere.

330 **Figure 4.** Lead-210 (black circles) and  $^{226}\text{Ra}$  (white circles) profiles against depth. Grey  
331 squares represent the  $^{210}\text{Pb}(\text{ex})$  profile vs cumulative dry mass.

332 **Figure 5.**  $\delta^{13}\text{C}$  vs  $\delta^{15}\text{N}$ . The Amazon River POM and Santarem soil organic matter values,  
333 adjacent to the study area, are taken from Zocatelli et al (2013).

334 **Figure 6.** Carbon burial as a function of  $\delta^{13}\text{C}$  and  $\delta^{15}\text{N}$ .

335 **Figure 7.**  $\delta^{13}\text{C}$ ,  $\delta^{15}\text{N}$  and carbon burial rate values in relation to depth (cm). Panels below  
336 each vertical profile represent respective data grouped by the three general phases >1930,  
337 1930-1970 and 1970-2010. Filled square symbols represent means of a given variable in  
338 each sediment layer, and the vertical bars show the mean with the standard deviation of the  
339 respective phase. Equal letters in each panel represent non-significant differences ( $p > 0.05$ ,  
340 one-way ANOVA followed by Tukey's post test).

341 **Figure 8.** Percentage of modified areas in relation to the different buffers (Panel A). Carbon  
342 burial (black dots) and changes in the riparian vegetation (two grey bars represent the two  
343 general phases) as related to time (Panel B).

344

345

346

347

#### 348 **CAPTION TO TABLES**

349 **Table 1.** Satellite acquisition data from United States Geological Survey (USGS) and the  
350 Curuá-Una River quota from Brazilian Water Agency (ANA).

351 **Table 2.** Depth profiles of dry bulk density (DBD), total organic carbon (OC%), total nitrogen  
352 (TN%) carbon and nitrogen (C/N) molar ratios,  $\delta^{13}\text{C}$  and  $\delta^{15}\text{N}$ .

353

354

355

356

357

358

359

360

361

362

363

364

365

366  
 367  
 368  
 369  
 370  
 371  
 372  
 373  
 374

**Table 1.**

<i>Month/Year</i>	<i>Landsat Data</i>	<i>Curuá-Una River Quote</i>
Aug/1975	2	5.3
Oct/1985	5	3.7
June/1995	5	6
June/2008	5	<i>No data</i>

375  
 376  
 377  
 378  
 379  
 380  
 381  
 382

**Table 2.**

<b>Depth (cm)</b>	<b>DBD (g cm<sup>-3</sup>)</b>	<b>δ<sup>15</sup>N</b>	<b>δ<sup>13</sup>C</b>	<b>C (%)</b>	<b>N (%)</b>	<b>C/N</b>
0-2	1.0	8.9	-29.2	3.8	0.3	17.2
2-4	0.9	11.7	-29.0	3.8	0.3	18.7
4-6	1.0	10.4	-28.8	4.0	0.3	19.2
6-8	1.1	9.3	-28.7	4.3	0.3	20.2
8-10	1.0	9.4	-28.7	4.1	0.3	19.8
10-12	1.1	7.9	-28.6	4.6	0.3	21.2
12-14	1.1	8.2	-28.7	4.3	0.3	19.9
14-16	1.1	7.8	-28.6	4.3	0.3	20.9
16-18	1.0	8.7	-28.5	4.4	0.3	21.2
18-20	1.1	7.5	-28.4	4.4	0.3	19.8
20-22	1.0	6.5	-28.2	5.4	0.3	21.2
22-24	1.0	6.0	-27.8	5.3	0.3	21.5
24-26	1.0	5.2	-27.4	7.3	0.4	25.4
26-28	1.1	6.1	-27.6	6.0	0.3	23.8
28-30	1.0	5.0	-27.3	6.0	0.4	22.7
30-32	1.0	5.4	-28.0	6.1	0.3	27.0
32-34	1.3	6.6	-28.5	4.4	0.2	27.5
34-36	1.6	8.9	-29.0	2.2	0.1	23.1
36-38	1.4	11.4	-29.4	2.9	0.1	30.4
38-40	1.4	10.4	-29.5	3.3	0.1	30.5
40-42	1.5	11.4	-29.3	2.4	0.1	23.8
42-44	1.6	12.2	-29.4	1.3	0.1	15.6
44-46	1.8	8.2	-29.6	1.2	0.1	14.3
46-48	1.5	8.8	-29.8	2.2	0.1	21.6
48-50	0.9	10.4	-29.7	2.9	0.2	25.6
50-52	0.9	10.2	-29.7	2.6	0.1	27.2
52-54	0.9	7.1	-29.7	3.9	0.2	28.6
54-56	0.9	9.2	-29.9	3.6	0.2	27.8
56-58	0.9	6.6	-30.1	4.3	0.2	30.1

58-60	0.9	5.0	-30.1	3.5	0.2	23.1
<b>Average</b>	<b>1.11</b>	<b>8.34</b>	<b>-28.9</b>	<b>4.0</b>	<b>0.2</b>	<b>23.0</b>
<b>Stand Dev</b>	<b>0.24</b>	<b>2.1</b>	<b>0.8</b>	<b>1.9</b>	<b>0.1</b>	<b>4.2</b>

## References

- 383  
384  
385 Aalto, R., L. Maurice-Bourgoin, T. Dunne, D. R. Montgomery, C. A. Nittrouer, and J. L.  
386 Guyot. 2003. Episodic sediment accumulation on Amazonian flood plains influenced  
387 by El Niño/Southern Oscillation. *Nature* **425**:493-497.
- 388 Abril, G., J. M. Martinez, L. F. Artigas, P. Moreira-Turcq, M. F. Benedetti, L. Vidal, T.  
389 Meziane, J. H. Kim, M. C. Bernardes, N. Savoye, J. Deborde, E. L. Souza, P. Albéric,  
390 M. F. Landim De Souza, and F. Roland. 2014. Amazon River carbon dioxide  
391 outgassing fuelled by wetlands. *Nature* **505**:395-398.
- 392 Amorim, A. T. d. S. 2000. Santarém: uma síntese histórica, Canoas, Ulbra, Santarem, Brazil
- 393 Anderson, N. J., R. D. Dietz, and D. R. Engstrom. 2013. Land-use change, not climate,  
394 controls organic carbon burial in lakes. *Proceedings. Biological sciences / The Royal*  
395 *Society* **280**:20131278.
- 396 Appleby, P. G., and F. Oldfield. 1992. Application of lead-210 to sedimentation studies.  
397 Pages 731-783 in M. Ivanovich and S. Harmon, editors. *Uranium Series*  
398 *Disequilibrium: Application to Earth, Marine and Environmental Science*. Oxford  
399 *Science Publications*.
- 400 Bakoariniaina, L. N., T. Kusky, and T. Raharimahefa. 2006. Disappearing Lake Alaotra:  
401 Monitoring catastrophic erosion, waterway silting, and land degradation hazards in  
402 Madagascar using Landsat imagery. *Journal of African Earth Sciences* **44**:241-252.
- 403 Brodie, C. R., J. S. L. Casford, J. M. Lloyd, M. J. Leng, T. Heaton, C. P. Kendrick, and Z.  
404 Yongqiang. 2011. Evidence for bias in C/N,  $\delta^{13}\text{C}$  and  $\delta^{15}\text{N}$  values of bulk organic  
405 matter, and on environmental interpretation, from a lake sedimentary sequence by  
406 pre-analysis acid treatment methods. *Quaternary Science Reviews* **30**:3076-3087.
- 407 Cohen, A. S., M. R. Palacios-Fest, J. McGill, P. W. Swarzenski, D. Verschuren, R. Sinyinza,  
408 T. Songori, B. Kakagozo, M. Syampila, C. M. O'Reilly, and S. R. Alin. 2005.  
409 Paleolimnological investigations of anthropogenic environmental change in Lake  
410 Tanganyika: I. An introduction to the project. *Journal of Paleolimnology* **34**:1-18.
- 411 Cruz, H., P. Sablayrolles, M. Kanashiro, and M. S. Amaral, P. 2011. Relação empresa/  
412 comunidade no manejo florestal comunitário e familiar: Uma contribuição do Projeto  
413 Floresta em pé.
- 414 Diaz, R. J., and R. Rosenberg. 2008. Spreading dead zones and consequences for marine  
415 ecosystems. *Science* **321**:926-929.
- 416 Dietz, R. D., D. R. Engstrom, and N. J. Anderson. 2015. Patterns and drivers of change in  
417 organic carbon burial across a diverse landscape: Insights from 116 Minnesota lakes.  
418 *Global Biogeochemical Cycles* **29**:708-727.
- 419 Dong, X., N. J. Anderson, X. Yang, X. chen, and J. Shen. 2012. Carbon burial by shallow  
420 lakes on the Yangtze floodplain and its relevance to regional carbon sequestration.  
421 *Global Change Biology* **18**:2205-2217.
- 422 Downing, J. P., M. Meybeck, J. C. Orr, R. R. Twilley, and H. W. Scharpenseel. 1993. Land  
423 and water interface zones. *Water, Air, & Soil Pollution* **70**:123-137.
- 424 Enea, A., G. Romanescu, and C. Stoleriu. 2012 Quantitative considerations concerning the  
425 source-areas for the silting of the red lake (Romania) lacustrine basin.  
426 . Romania.
- 427 Fearnside, P. M. 2005. Do hydroelectric dams mitigate global warming? The case of Brazil's  
428 Curuá-Una Dam. *Mitigation and Adaptation Strategies for Global Change* **10**:675-  
429 691.



430 Gordon, S. I. 1980. Utilizing LANDSAT imagery to monitor land-use change: A case study  
431 in ohio. *Remote Sensing of Environment* **9**:189-196.

432 Goulding, M. 1993. Flooded forests of the Amazon. *Scientific American* **268**:114-120+115.

433 Hoffmann, T., M. Schlummer, B. Notebaert, G. Verstraeten, and O. Korup. 2013. Carbon  
434 burial in soil sediments from Holocene agricultural erosion, Central Europe. *Global*  
435 *Biogeochemical Cycles* **27**:828-835.

436 INPE. 2016. Program for the Estimation of Amazon Deforestation. Accessed 20 November  
437 2016, [http://www.obt.inpe.br/prodes/prodes\\_1988\\_2015n.htm](http://www.obt.inpe.br/prodes/prodes_1988_2015n.htm).

438 Ivanovich, M., and S. Harmon. 1992. Uranium Series Disequilibrium - Applications to Earth,  
439 Marine and Environmental Sciences. second edition edition. Oxford Science  
440 Publications.

441 Junk, W. J. 2013. Current state of knowledge regarding South America wetlands and their  
442 future under global climate change. *Aquatic Sciences* **75**:113-131.

443 Ketterer, M. E., K. M. Hafer, V. J. Jones, and P. G. Appleby. 2004. Rapid dating of recent  
444 sediments in Loch Ness: Inductively coupled plasma mass spectrometric  
445 measurements of global fallout plutonium. *Science of the Total Environment*  
446 **322**:221-229.

447 Ligocki, L. P. 2003. Comportamento geotécnico da barragem de Curuá-Una, Pará. Rio de  
448 Janeiro.

449 Lucas, C. M., J. Schöngart, P. Sheikh, F. Wittmann, M. T. F. Piedade, and D. G. McGrath.  
450 2014. Effects of land-use and hydroperiod on aboveground biomass and productivity  
451 of secondary Amazonian floodplain forests. *Forest Ecology and Management*  
452 **319**:116-127.

453 Marotta, H., L. Bento, F. A. De Esteves, and A. Enrich-Prast. 2009. Whole ecosystem  
454 evidence of eutrophication enhancement by wetland dredging in a shallow Tropical  
455 Lake. *Estuaries and Coasts* **32**:654-660.

456 Marotta, H., C. M. Duarte, F. Meirelles-Pereira, L. Bento, F. A. Esteves, and A. Enrich-Prast.  
457 2010. Long-term CO<sub>2</sub> variability in two shallow tropical lakes experiencing episodic  
458 eutrophication and acidification events. *Ecosystems* **13**:382-392.

459 Marotta, H., L. Pinho, C. Gudas, D. Bastviken, L. J. Tranvik, and A. Enrich-Prast. 2014.  
460 Greenhouse gas production in low-latitude lake sediments responds strongly to  
461 warming. *Nature Climate Change* **4**:467-470.

462 Melack, J. M., L. L. Hess, M. Gastil, B. R. Forsberg, S. K. Hamilton, I. B. T. Lima, and E. M.  
463 L. M. Novo. 2004. Regionalization of methane emissions in the Amazon Basin with  
464 microwave remote sensing. *Global Change Biology* **10**:530-544.

465 Munyati, C. 2000. Wetland change detection on the Kafue Flats, Zambia, by classification of  
466 a multitemporal remote sensing image dataset. *International Journal of Remote*  
467 *Sensing* **21**:1787-1806.

468 Naidu, A. S., L. W. Cooper, B. P. Finney, R. W. Macdonald, C. Alexander, and I. P.  
469 Semiletov. 2000. Organic carbon isotope ratio ( $\delta^{13}C$ ) of Arctic Amerasian  
470 Continental shelf sediments. *International Journal of Earth Sciences* **89**:522-532.

471 Neill, C., M. T. Coe, S. H. Riskin, A. V. Krusche, H. Elsenbeer, M. N. Macedo, R.  
472 McHorney, P. Lefebvre, E. A. Davidson, R. Scheffler, A. M. e Silva Figueira, S.  
473 Porder, and L. A. Deegan. 2013a. Watershed responses to Amazon soya bean  
474 cropland expansion and intensification. *Philosophical Transactions of the Royal*  
475 *Society B: Biological Sciences* **368**.

476 Neill, C., M. T. Coe, S. H. Riskin, A. V. Krusche, H. Elsenbeer, M. N. Macedo, R.  
477 McHorney, P. Lefebvre, E. A. Davidson, R. Scheffler, A. M. Figueira, S. Porder, and  
478 L. A. Deegan. 2013b. Watershed responses to Amazon soya bean cropland expansion

479 and intensification. Philosophical transactions of the Royal Society of London. Series  
480 B, Biological sciences **368**:20120425.

481 Neue, H. U., J. L. Gaunt, Z. P. Wang, P. Becker-Heidmann, and C. Quijano. 1997. Carbon in  
482 tropical wetlands. *Geoderma* **79**:163-185.

483 Ometto, J. P. H. B., J. R. Ehleringer, T. F. Domingues, J. A. Berry, F. Y. Ishida, E. Mazzi, N.  
484 Higuchi, L. B. Flanagan, G. B. Nardoto, and L. A. Martinelli. 2006. The stable carbon  
485 and nitrogen isotopic composition of vegetation in tropical forests of the Amazon  
486 Basin, Brazil. *Biogeochemistry* **79**:251-274.

487 Peixoto, R. B., H. Marotta, D. Bastviken, and A. Enrich-Prast. 2016. Floating Aquatic  
488 Macrophytes Can Substantially Offset Open Water CO<sub>2</sub> Emissions from  
489 Tropical Floodplain Lake Ecosystems. *Ecosystems* **19**:724-736.

490 Sanders, C. J., B. D. Eyre, I. R. Santos, W. MacHado, W. Luiz-Silva, J. M. Smoak, J. L.  
491 Breithaupt, M. E. Ketterer, L. Sanders, H. Marotta, and E. Silva-Filho. 2014. Elevated  
492 rates of organic carbon, nitrogen, and phosphorus accumulation in a highly impacted  
493 mangrove wetland. *Geophysical Research Letters* **41**:2475-2480.

494 Sanders, C. J., I. R. Santos, D. T. Maher, J. L. Breithaupt, J. M. Smoak, M. Ketterer, M. Call,  
495 L. Sanders, and B. D. Eyre. 2016. Examining <sup>239+240</sup>Pu, <sup>210</sup>Pb and historical events  
496 to determine carbon, nitrogen and phosphorus burial in mangrove sediments of  
497 Moreton Bay, Australia. *Journal of Environmental Radioactivity* **151**:623-629.

498 Sanders, L. M., K. H. Taffs, D. J. Stokes, C. J. Sanders, J. M. Smoak, A. Enrich-Prast, P.  
499 Macklin, I. R. Santos, and H. Marotta. 2017. Carbon accumulation in Amazonian  
500 floodplain lakes: A significant component of Amazon budgets? *Limnology &  
501 Oceanography Letters*:29-35.

502 Skole, D., and C. Tucker. 1993. Tropical deforestation and habitat fragmentation in the  
503 amazon: Satellite data from 1978 to 1988. *Science* **260**:1905-1910.

504 Smith, L. K., J. M. Melack, and D. E. Hammond. 2002. Carbon, nitrogen, and phosphorus  
505 content and <sup>210</sup>Pb-derived burial rates in sediments of an Amazon floodplain lake.  
506 *Amazoniana* **17**:413-436.

507 Stanley, E. H., S. M. Powers, N. R. Lottig, I. Buffam, and J. T. Crawford. 2012.  
508 Contemporary changes in dissolved organic carbon (DOC) in human-dominated  
509 rivers: Is there a role for DOC management? *Freshwater Biology* **57**:26-42.

510 Zocatelli, R., P. Moreira-Turcq, M. Bernardes, B. Turcq, R. C. Cordeiro, S. Gogo, J. R.  
511 Disnar, and M. Boussafir. 2013. Sedimentary evidence of soil organic matter input to  
512 the curuai amazonian floodplain. *Organic Geochemistry* **63**:40-47.

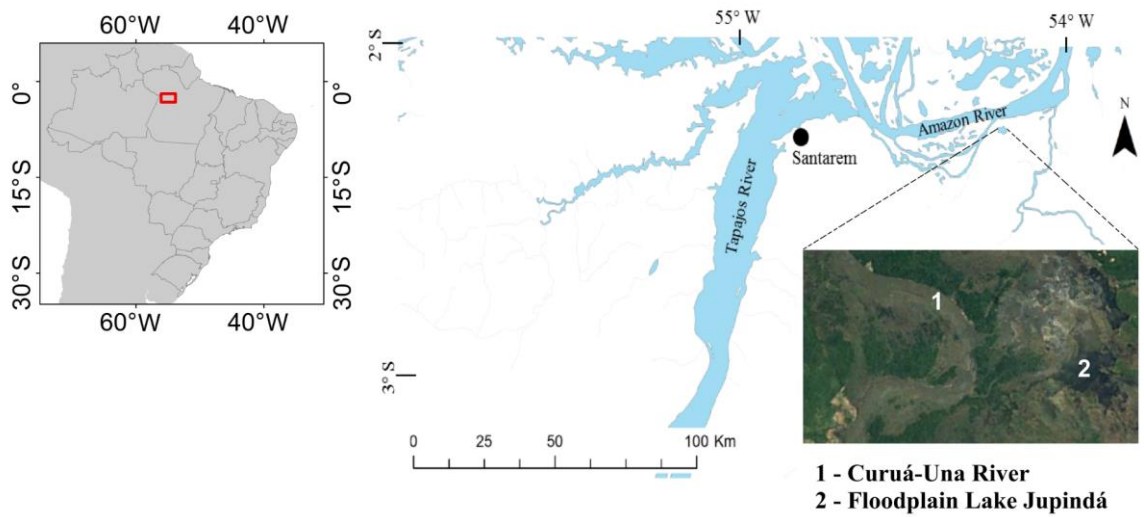
513

514

515

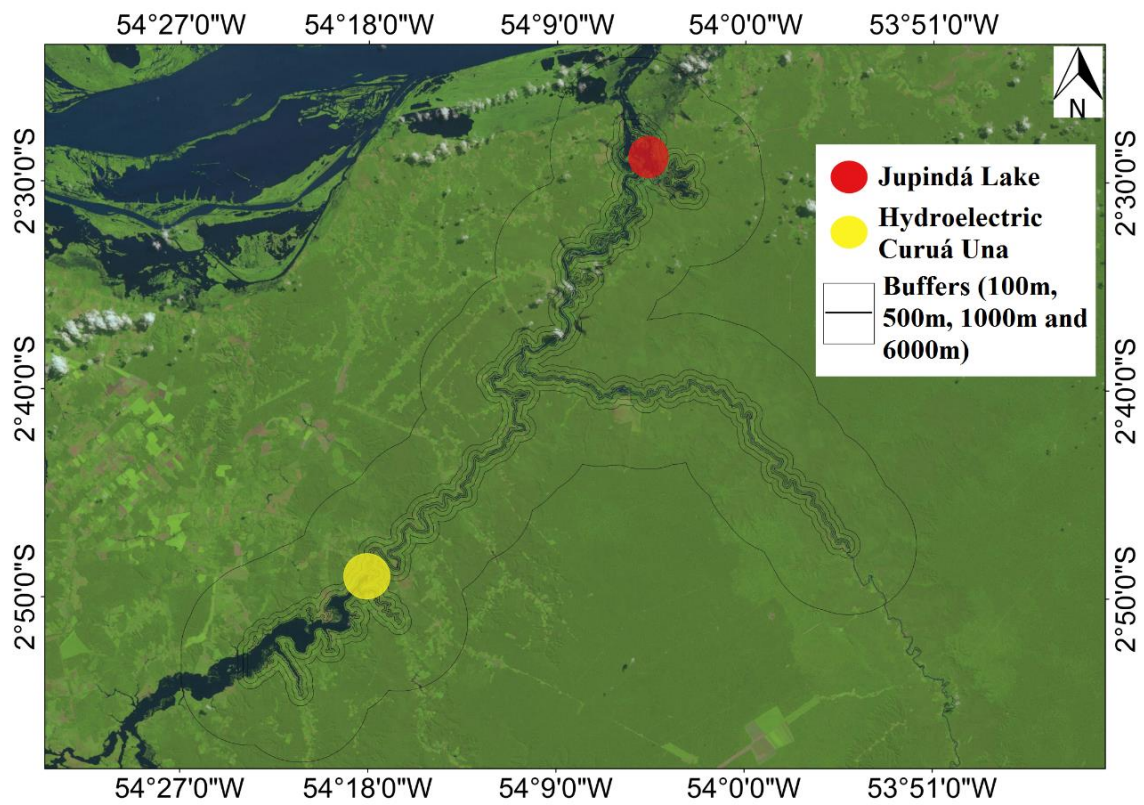
516

517 **Figure 1.**



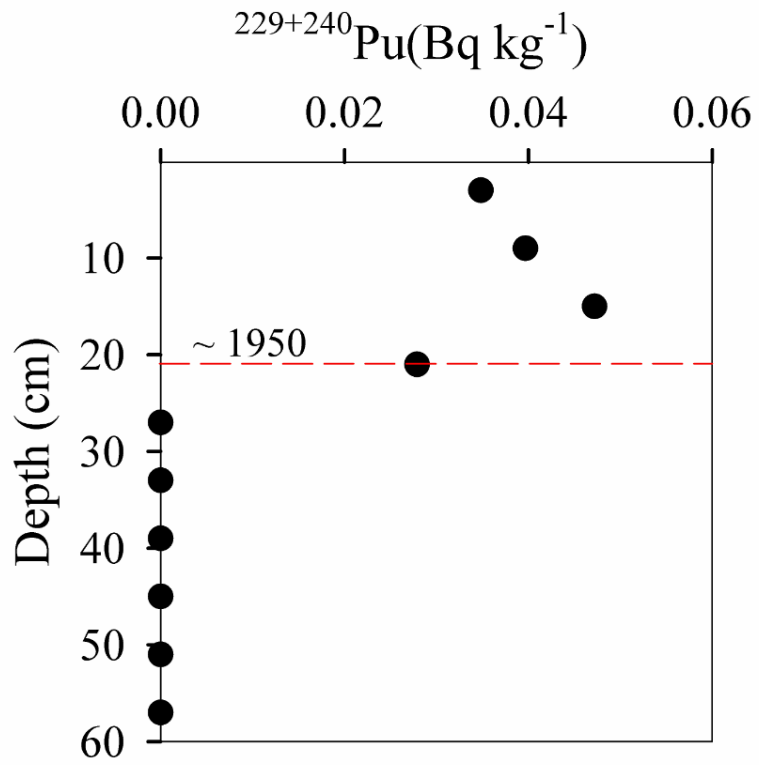
518  
 519  
 520  
 521  
 522  
 523  
 524  
 525  
 526  
 527  
 528  
 529  
 530  
 531  
 532  
 533  
 534  
 535  
 536  
 537  
 538  
 539  
 540  
 541  
 542  
 543  
 544  
 545  
 546  
 547  
 548  
 549

**Figure 2.**



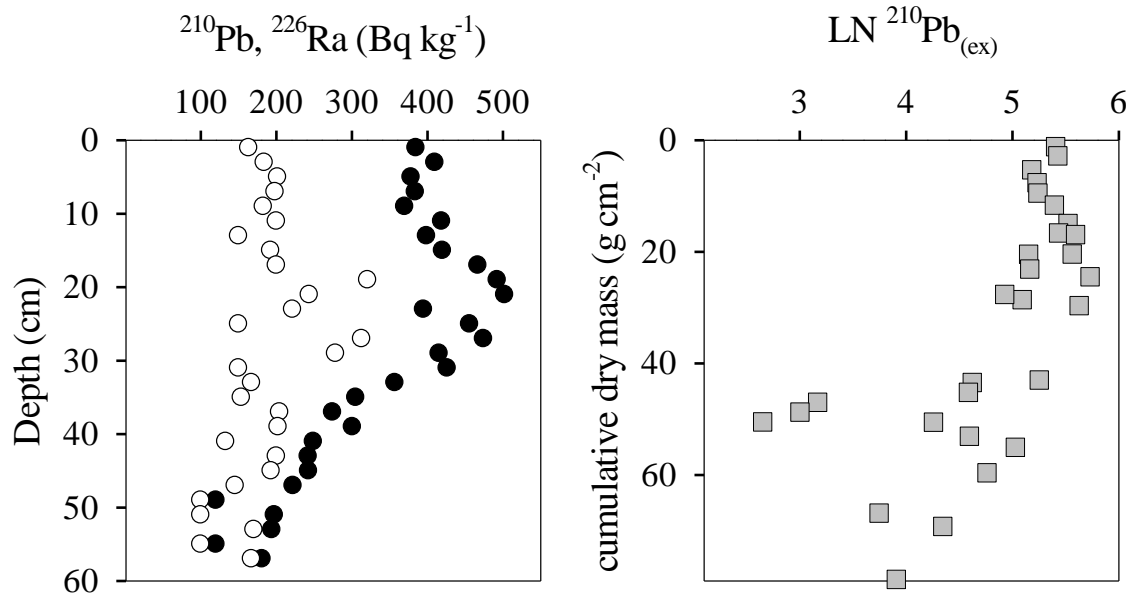
550  
 551  
 552  
 553  
 554  
 555  
 556  
 557  
 558  
 559  
 560  
 561  
 562  
 563  
 564  
 565  
 566  
 567  
 568  
 569  
 570  
 571  
 572  
 573  
 574

**Figure 3.**



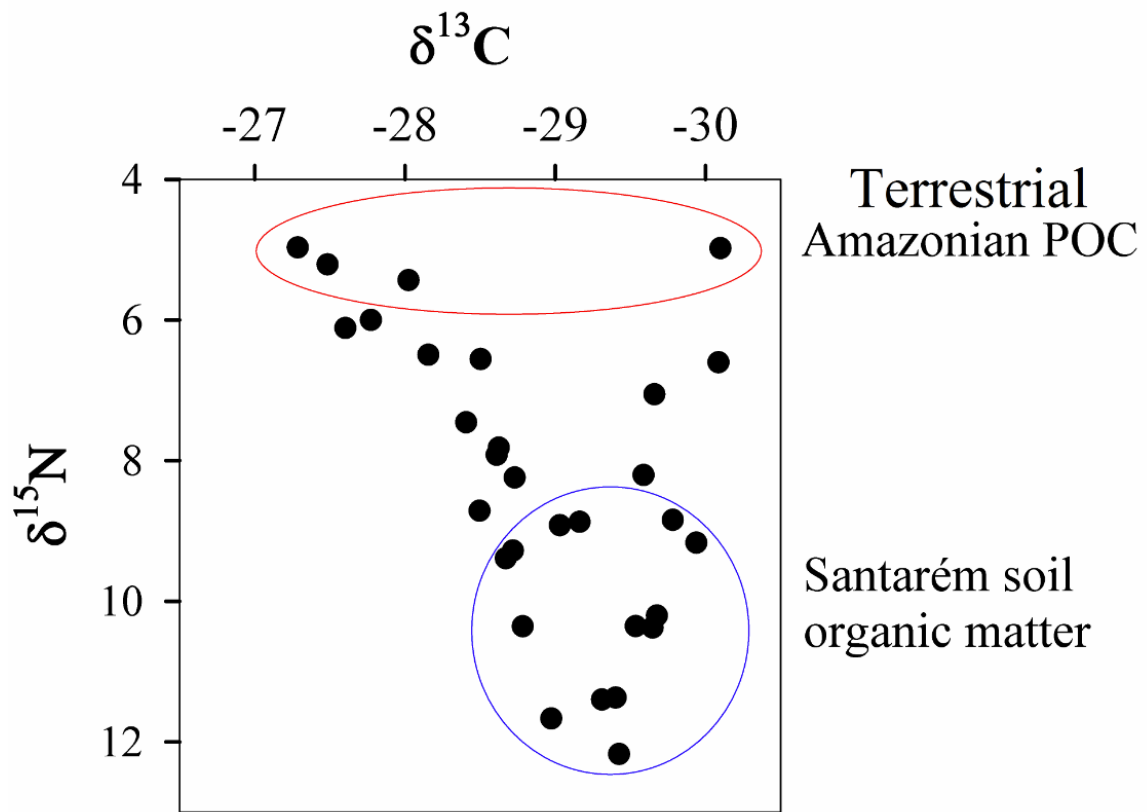
575  
 576  
 577  
 578  
 579  
 580  
 581  
 582  
 583  
 584  
 585  
 586  
 587  
 588  
 589  
 590  
 591  
 592  
 593  
 594  
 595  
 596  
 597  
 598  
 599  
 600

Figure 4.



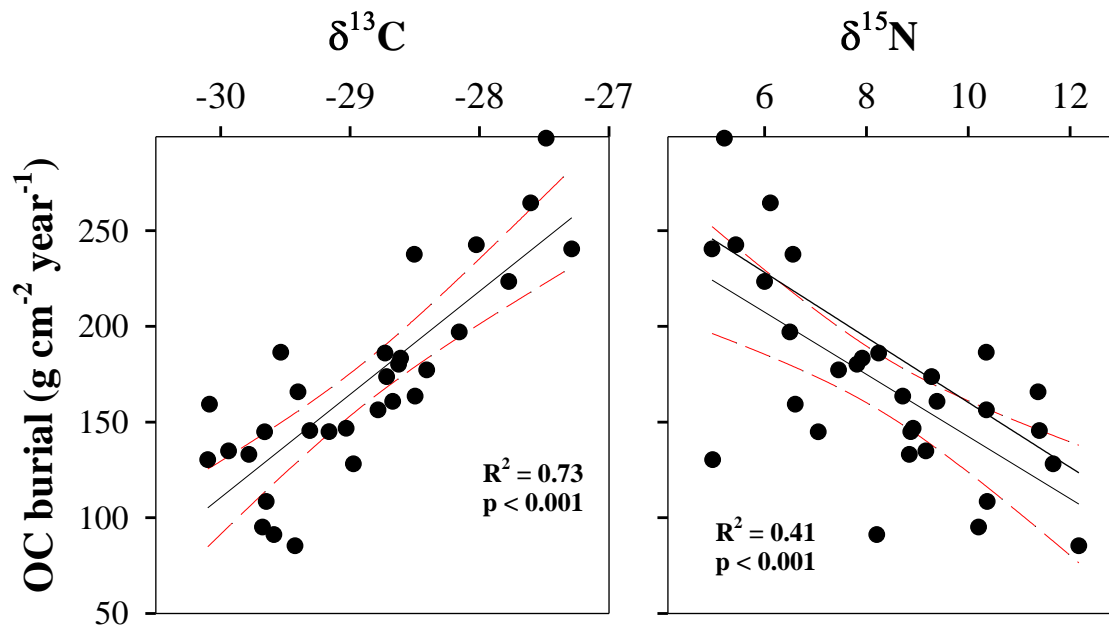
601  
 602  
 603  
 604  
 605  
 606  
 607  
 608  
 609  
 610  
 611  
 612  
 613  
 614  
 615  
 616  
 617  
 618  
 619  
 620  
 621  
 622  
 623  
 624  
 625  
 626  
 627  
 628  
 629  
 630

**Figure 5.**



631  
 632  
 633  
 634  
 635  
 636  
 637  
 638  
 639  
 640  
 641  
 642  
 643  
 644  
 645  
 646  
 647  
 648  
 649  
 650  
 651  
 652  
 653  
 654

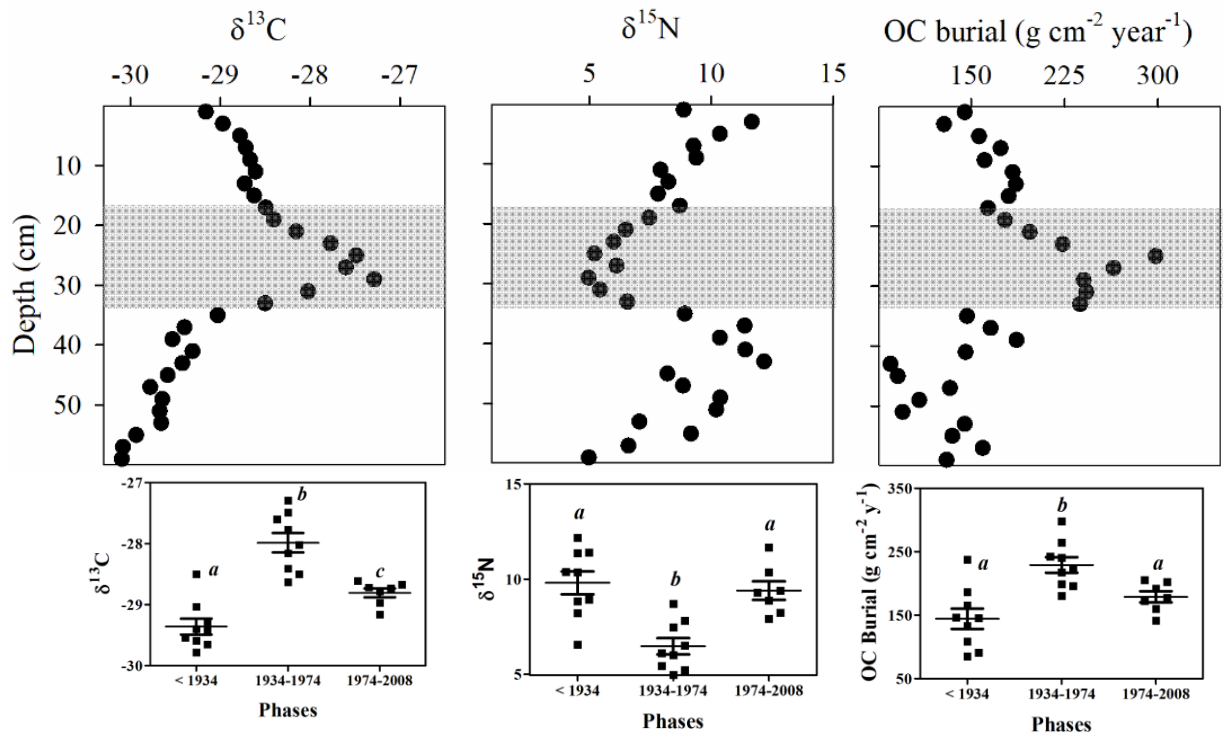
**Figure 6.**



655  
 656  
 657  
 658  
 659  
 660  
 661  
 662  
 663  
 664  
 665  
 666  
 667  
 668  
 669  
 670  
 671  
 672  
 673  
 674  
 675  
 676  
 677  
 678  
 679  
 680  
 681  
 682  
 683

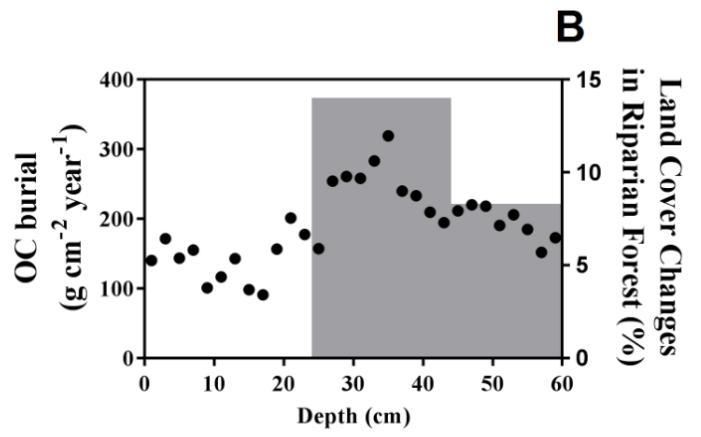
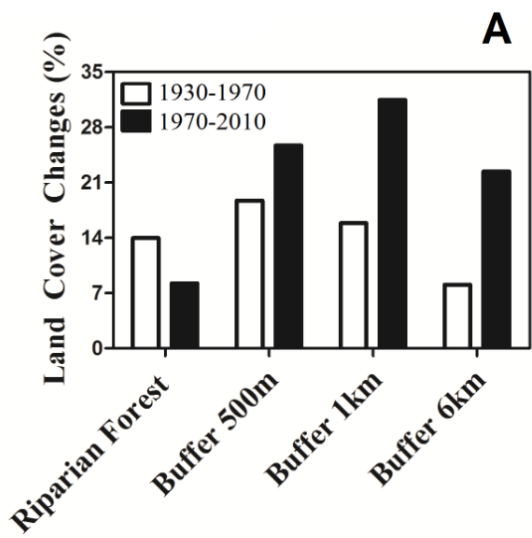
**Figure 7.**





684  
 685  
 686  
 687  
 688  
 689  
 690  
 691  
 692  
 693  
 694  
 695  
 696  
 697  
 698  
 699  
 700  
 701  
 702  
 703  
 704  
 705  
 706  
 707  
 708  
 709  
 710

**Figure 8.**



711  
712